Electronic Supplementary Material (ESI) for Green Chemistry.

Supporting Information

L-Lysine-induced green synthesis of CoS/Co_3O_4 nanoframes for efficient electrocatalytic oxygen evolution

Jinrui Hu,[a] Zhijuan Li,*[b] Dongsheng Zhao,[a] Zheng Han,[a] Xiangrui Wu,[a] Jiayu Zhai,[b] Zhenyuan Liu,[c] Yawen Tang,*[a] Gengtao Fu*[a]

[a] Jiangsu Key Laboratory of New Power Batteries, Jiangsu Collaborative Innovation Centre of Biomedical Functional Materials, School of Chemistry and Materials Science, Nanjing Normal University, Nanjing 210023, China.

E-mail: gengtaofu@njnu.edu.cn (G. Fu); tangyawen@njnu.edu.cn (Y. Tang)

[b] School of Environmental Science, Nanjing Xiaozhuang University, Nanjing 211171, China.

E-mail:zhijuanlibbd@163.com (Z. Li).

[c] School of Materials Science and Engineering, Jiangsu University of Science and Technology, Zhenjiang 212100, China.

Experimental

Reagents and chemicals

Cobalt(II) acetate tetrahydrate ($Co(AC)_2 \cdot 4H_2O$), l-lysine ($C_6H_{14}N_2O_2$), thioacetamide (TAA) and commercial Ruthenium oxide (RuO_2) were purchased from Aladdin Chemistry Co., Ltd (Shanghai China). 20% Pt/C was purchased from Johnson Matthey Corporation. Sodium hydroxide (NaOH), potassium hydroxide (KOH) and ethanol (C_2H_5OH) were purchased from Sinopharm Chemical Reagent Co., Ltd (Shanghai, China). All the reagents were of analytical reagent grade and used without further purification.

Samples preparation

For the synthesis of $Co(OH)_2$ NSs, 8 mg of $Co(AC)_2 \cdot 4H_2O$ and 100 mg of $C_6H_{14}N_2O_2$ solid powder were weighed into 12.5 mL of deionized (DI) water, and a homogeneous solution of clarification was formed after sufficient ultrasonication. Subsequently, the solution was rapidly adjusted to pH=13.3 with concentrated NaOH solution, and stirred for 20 min. Afterward, the prepared solution was transferred into a 25 mL Teflon-lined stainless-steel autoclave, which was maintained at 180 °C for 12 h before cooling down to room temperature. The product obtained by centrifugation was named the $Co(OH)_2$ NRs and washed with ethanol several times and then dried at 60 °C.

For the synthesis of CoS/Co_3O_4 NFs, 10 mg of $Co(OH)_2$ NSs and 50 mg of TAA were dissolved in 12.5 mL of ethanol by sonication and stirred for 1 h. Then, the prepared solution was transferred into a 25 mL Teflon-lined stainless-steel autoclave, which was maintained at 120 °C for 5 h before cooling down to room temperature. The solution was centrifuged and washed several times with a mixed solution of ethanol and DI, and dried to obtain the CoS/Co_3O_4-5 NFs. Whereafter, while keeping other experimental conditions and the mass of the precursor unchanged, only the mass of TAA was changed to 20 mg and 100 mg, respectively, to obtain the CoS/Co_3O_4-2 NFs and CoS/Co_3O_4-10 NFs after vulcanization, respectively.

For the synthesis of Co_3O_4, the pure Co_3O_4 was prepared by using the prepared $Co(OH)_2$ NSs at 300 ^oC with a heating rate of 2 ^oC/min for 2 h under an air atmosphere. For the synthesis of CoS, 5 mg of the as-prepared Co_3O_4 and 25 mg CH_4N_2S were placed in a porcelain boat at the downstream and upstream sides of the tube furnace respectively. Then, the porcelain boat was heated to 450 °C with a ramp rate of 2 °C/min for 1 h under Ar-H_2 atmosphere.

Characterization

X-ray powder diffraction (XRD) patterns were processed on a D/max-rC X-ray diffractometer. Specifically, Cu Kα (λ = 1.5406 A) was used as the radiation source and manipulated at 40 kV and 100 mA. Transmission electron microscopy (TEM), high-resolution transmission electron microscopy (HRTEM), high angle annular dark-field scanning transmission electron microscopy (HAADF-STEM), and energy-dispersive X-ray spectrum (EDX) were acquired on JEOL JEM-2100F and JEM-1400 with an accelerating voltage of 200 Kv and 80 Kv, respectively. Thermogravimetric analysis (TGA) was carried out under air with a temperature ramp of 10 ◦C/ min using a Netzsch SSTA 449C thermogravimetric analyzer (Netzsch STA 449C). The electron spin resonance (ESR) analysis of •OH trapped by DMPO was obtained on a JEOL spectrometer (JES-FA200) at ambient temperature. Scanning electron microscopy (SEM) was conducted on a Hitachi S4800 and Thermo Scientific color SEM Apreo 2S scanning electron microscopy. X-ray photoelectron spectroscopy (XPS) data were recorded on Thermo VG Scientific ESCALAB 250 spectrometer with an Al Kα light source. Brunauer-Emmett-Teller (BET) specific surface area and pore size distribution were carried out under 77.3 K with a Micromeritics ASAP 2020 system.

Electrochemical measurements

All electrochemical tests were carried out on a CHI 760E electrochemical analyzer at room temperature (25 ^{o}C), in a three-electrode system consisting of a glassy carbon electrode (GCE, d = 3 mm) as the working electrode, a saturated calomel electrode (SCE) as the reference electrode, and a graphite rod as the counter electrode. Then, the surface of the GCE electrode was modified by adding 5 μL of the prepared catalyst test solution twice and 3 μl of 20 % Nafion solution once. Polarization curves of OER were obtained at room temperature under test conditions at a scan rate of 5 mV s^{-1} in an O_2 saturated 1.0 M KOH solution. The electrochemical bilayer capacitance (C_{dl}) was obtained by a series of CV tests (scan rate 20 to 100 mV s^{-1}) in the potential range of 1.02 to 1.12 V (vs. RHE). All electric potentials were converted to reversible hydrogen electrodes (RHE) according to the following formula: ERHE = ESCE + 0.0592pH + 0.242.

Zn-air battery tests

The liquid Zn-air battery tests were conducted in a homemade Zn-air cell. The air cathode consists of porous carbon paper with a gas diffusion layer (GDL). The mixed solution of 0.2 M $ZnCl_2$ and 6 M KOH was used as an

alkaline electrolyte solution for a rechargeable Zn-air battery. The electrocatalyst solution for Zn-air battery tests was obtained by dissolving 10 mg of electrocatalyst in a mixed solution composed of 100 µL H_2O, 100 µL ethanol and 50 µL Nafion. The Lan CT2001A system was used for the battery test, and the discharge test was carried out under different current densities and specific capacities of the electrocatalyst samples. Each discharge cycle was set to 10 min. Additionally, the battery test for open-circuit potential (OCP) and power density was performed on the CHI 760E electrochemical analyzer system.

Theoretical calculations

Density functional theory (DFT) calculations were operated with Vienna *ab initio* Simulation Package (VASP),[1, 2] employing the generalized gradient approximation (GGA) with the Perdew-Burke-Ernzerhof (PBE) functional. The interaction for core electrons was depicted by the projector augmented wave (PAW) method[3]. Valence electrons were described by expanding the Kohn-Sham wavefunctions with plane-wave basis set with the energy cutoff of 450 eV. The convergence for all the forces on each atom was determined to be lower than 0.03 eV/Å. For bulk Co_3O_4 and CoS calculation, the Monkhorst-Pack[4] *k*-point grid sampling for the first Brillouin zone was 4×4×4 and 6×6×6 respectively. For slab model, the Co_3O_4 (110) and CoS (001) were achieved for investigation. The description for van deer Waals interaction used the DFT-D3 method proposed by Grimme et al[5] with zero-damping function. The strong on-site interaction for the Co-3d electrons was treated by DFT+U method as Hubbard model, where the effective U value for Co-3d was 3 eV according to Dudarev et al.[6] The self-convergence for electronic energy was below 10^{-5} eV.

Figures and tables

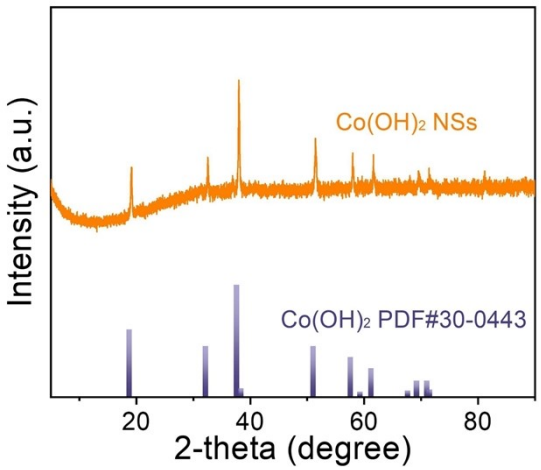

Fig. S1 XRD pattern of $Co(OH)_2$ NSs.

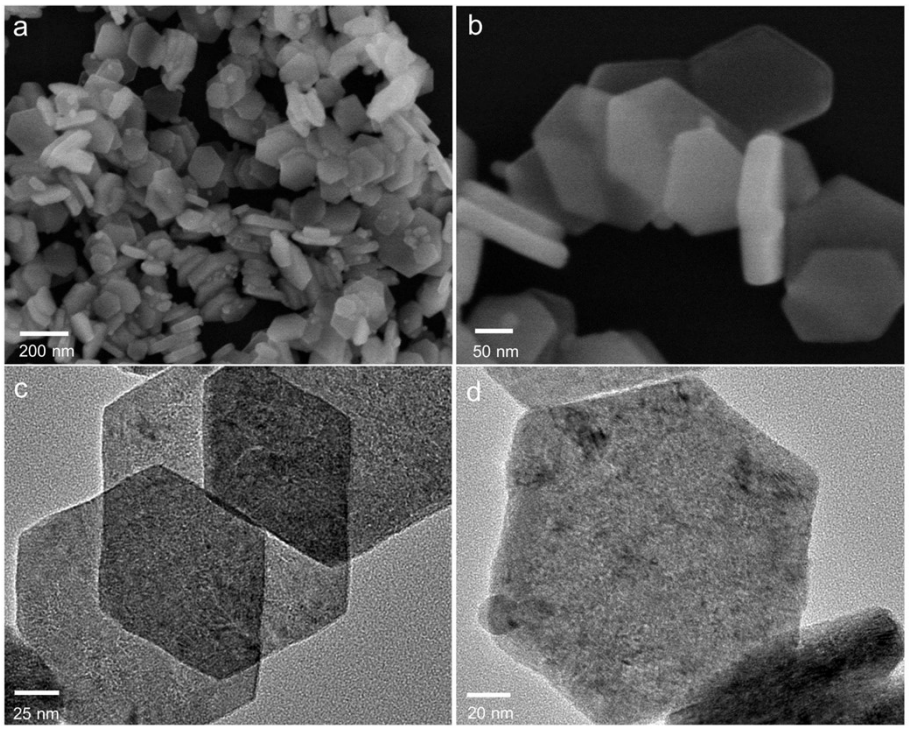

Fig. S2 (a-b) SEM images of $Co(OH)_2$ NSs; (c-d) TEM images of $Co(OH)_2$ NSs.

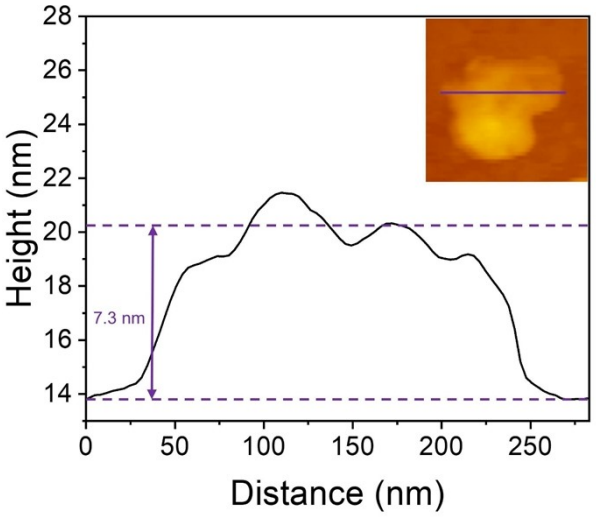

Fig. S3 AFM image of $Co(OH)_2$ NSs.

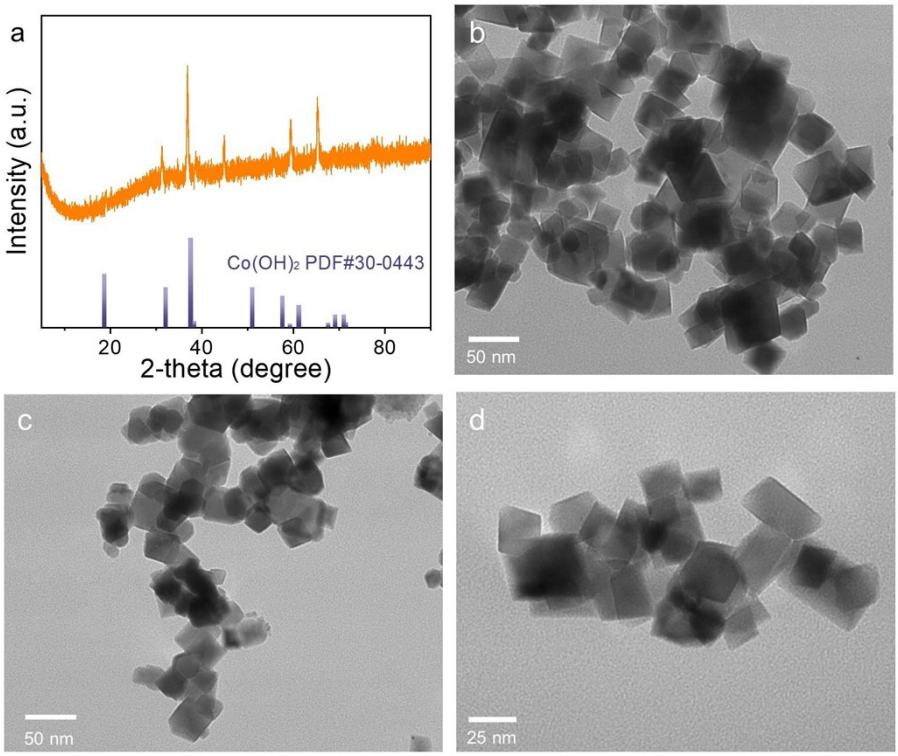

Fig. S4 (a) XRD pattern and (b-d) TEM images of the $Co(OH)_2$ nanoparticles in the absence of L-lysine.

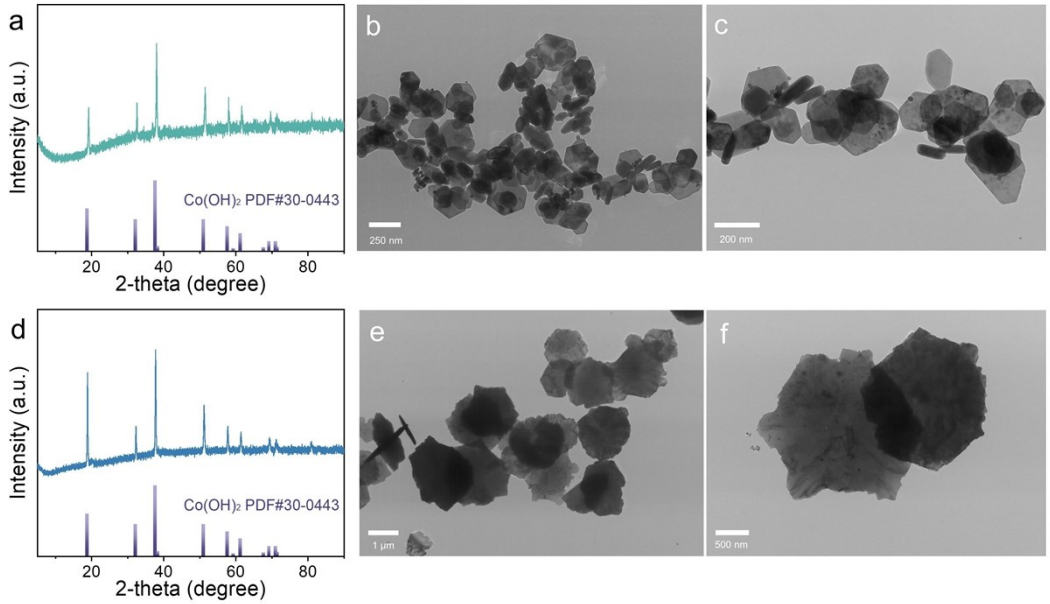

Fig. S5 (a) XRD pattern and (b-c) TEM images of the $Co(OH)_2$ precursor with 50 mg of L-lysine; (d) XRD pattern and (e-f) TEM images of the $Co(OH)_2$ precursor with 150 mg of L-lysine.

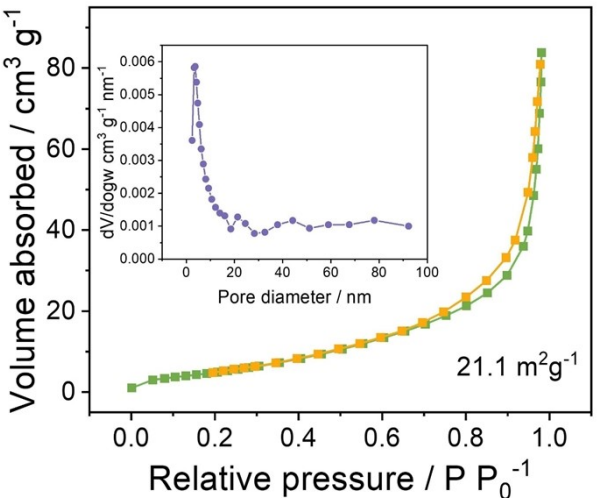

Fig. S6 N_2 adsorption-desorption isotherms and Pore-size distribution of CoS/Co_3O_4 NFs.

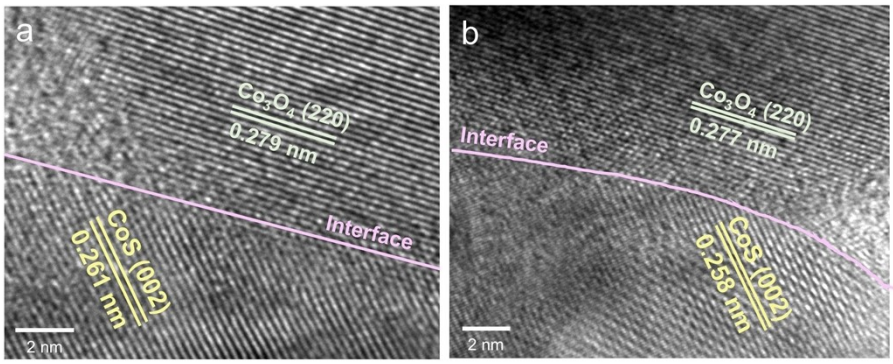

Fig. S7 HRTEM images of CoS/Co_3O_4 NFs.

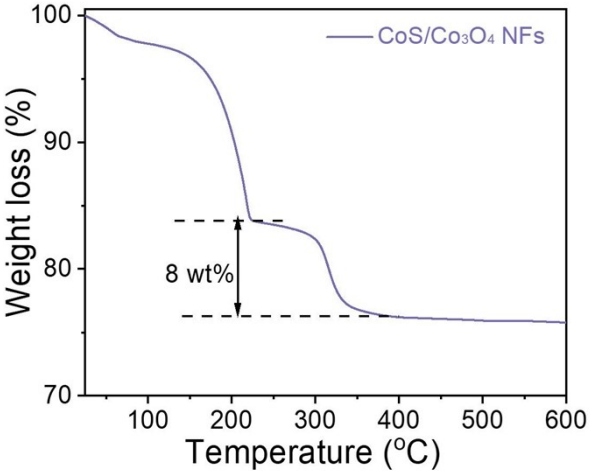

Fig. S8 TGA curve of CoS/Co_3O_4 NFs sample.

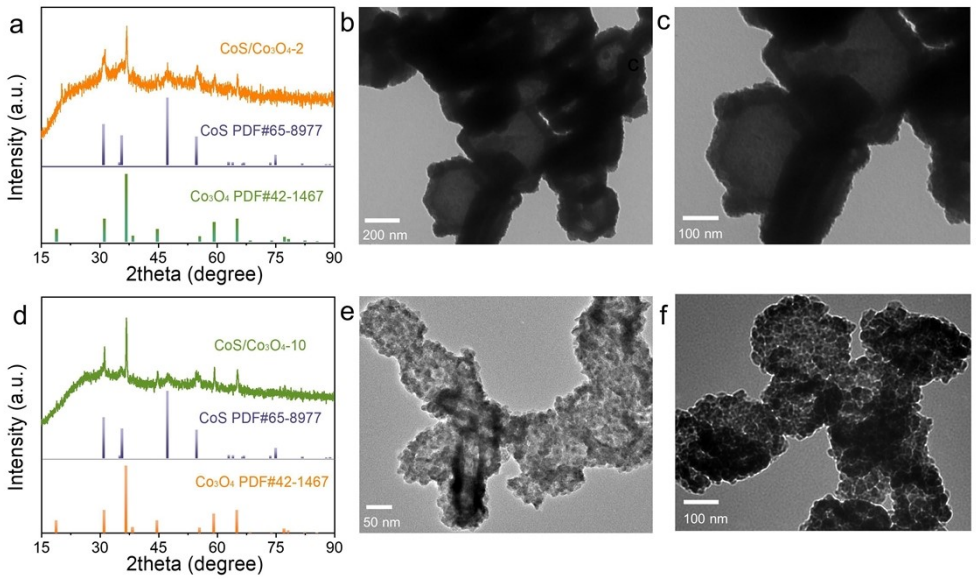

Fig. S9 (a) XRD pattern and (b-c) TEM images of CoS/Co_3O_4-2; (d) XRD pattern and (e-f) TEM images of CoS/Co_3O_4-10.

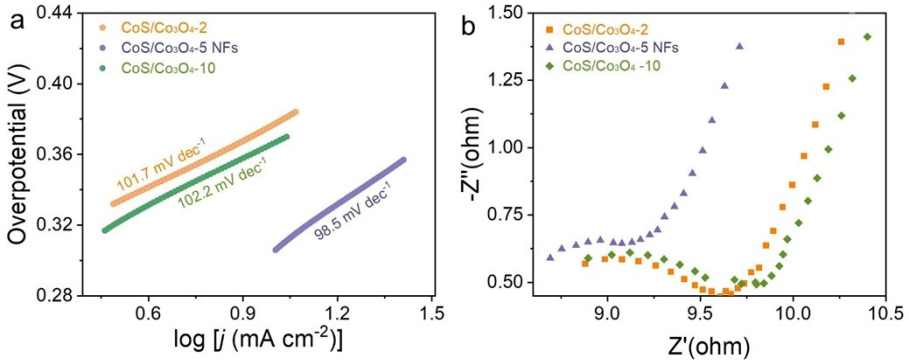

Fig. S10 Comparison of the OER activity of CoS/Co_3O_4-2, CoS/Co_3O_4-5 NFs and CoS/Co_3O_4-10: (a) Tafel plots derived from the panel Fig.3a; (b) EIS Nyquist plots.

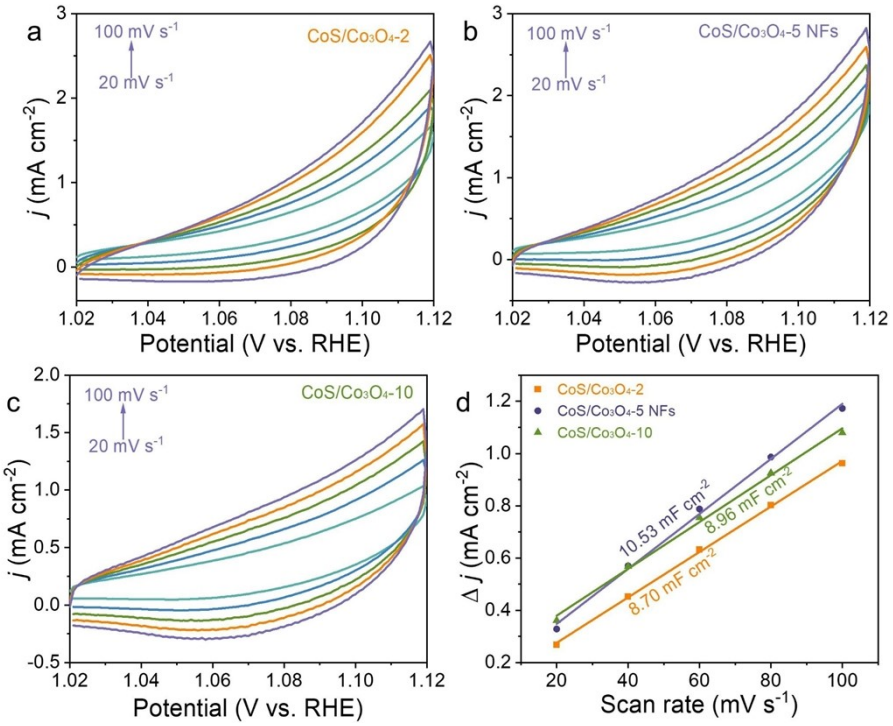

Fig. S11 (a-c) CV curves of catalysts in the non-Faradaic region (-1-1.1 V) obtained at different scanning rates of CoS/Co_3O_4-2, CoS/Co_3O_4-5 NFs and CoS/Co_3O_4-10; (d) C_{dl} values of catalysts.

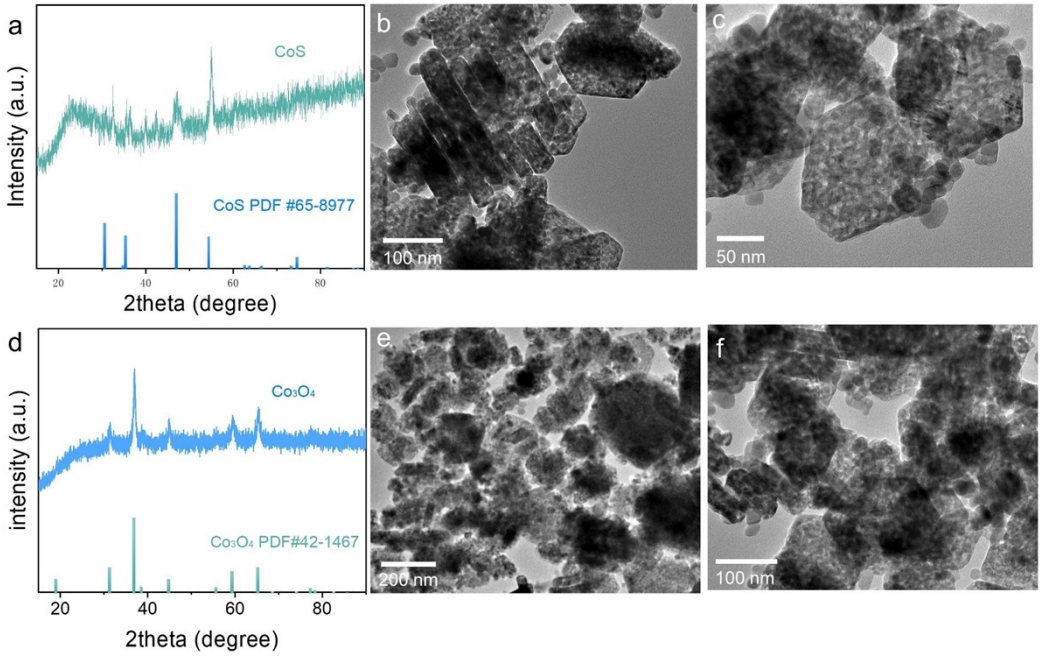

Fig. S12 (a) XRD pattern and (b-c) TEM images of CoS; (d) XRD pattern and (e-f) TEM images of Co_3O_4.

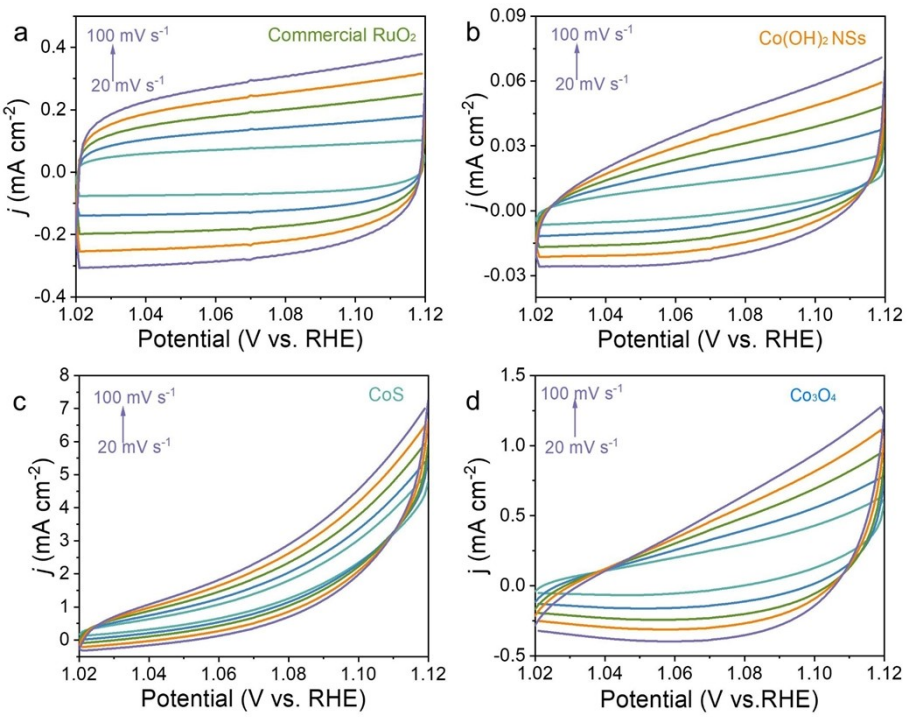

Fig. S13 CV curves of the synthesized catalysts in the non-Faradaic region (-1-1.1 V) were obtained at different scanning rates. (a) Commercial RuO_2; (b) $Co(OH)_2$ NSs; (c) CoS; (d) Co_3O_4.

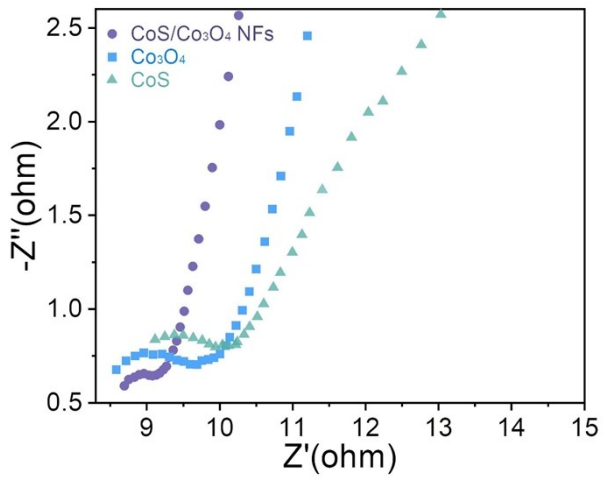

Fig. S14 EIS Nyquist plots of CoS/Co_3O_4 NFs, Co_3O_4 and CoS.

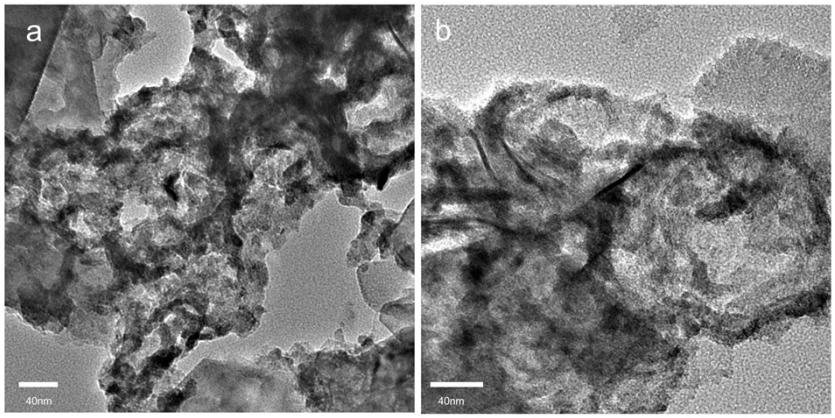

Fig. S15 TEM images of CoS/Co_3O_4 NFs after the OER.

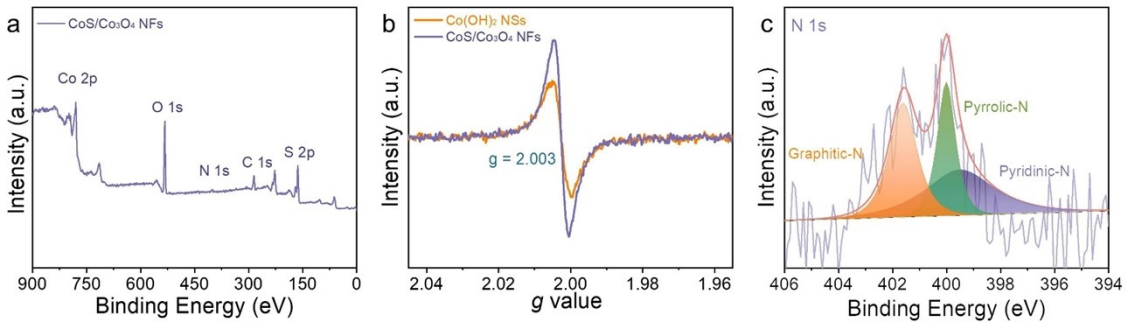

Fig. S16 (a) Full XPS spectra of CoS/Co_3O_4 NFs; (b)ESR spectra of CoS/Co_3O_4 NFs and $Co(OH)_2$ NSs; (c) High-resolution N 1s XPS spectra of CoS/Co_3O_4 NFs.

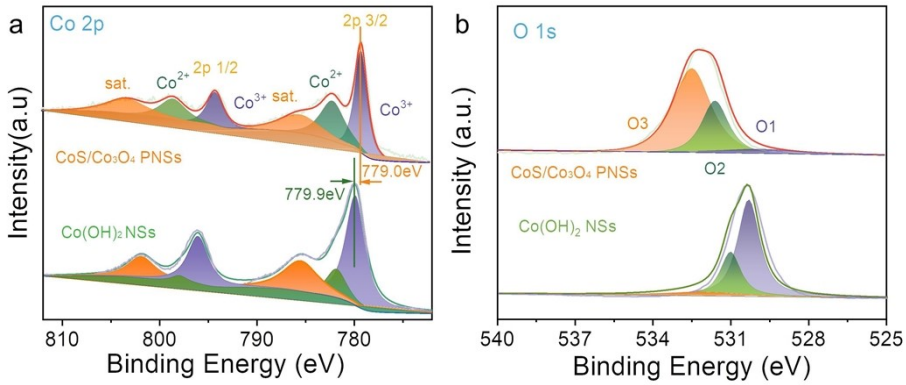

Fig. S17 (a) High-resolution Co 2p XPS spectra and (b) High-resolution O 1s XPS spectra of CoS/Co_3O_4 NFs and $Co(OH)_2$ NSs.

Table S1. OER Comparison of CoS/Co_3O_4 NFs with other Co-based catalysts reported before.

Catalyst	Electrolyte	E_{j10} / mV	Ref.
CoS/Co_3O_4 NFs	1.0 M KOH	304	This work
$Co(OH)_2$ NSs	1.0 M KOH	390	This work
CoS	1.0 M KOH	435	This work
Co_3O_4	1.0 M KOH	536	This work
$CoNC-NB_2$	1.0 M KOH	350	[7]
Ni-Co-P nanoboxes	1.0 M KOH	330	[8]
Co/CoO	1.0 M KOH	350	[9]
Co/CoP-5	1.0 M KOH	340	[10]
ferromagnetic $FeCo_2O_4$ nanofibers	1.0 M KOH	310	[11]
FeCo-NC	1.0 M KOH	343	[12]
$V-Co_9S_8$	1.0 M KOH	380	[13]

Table S2. Comparison of power density of CoS/Co_3O_4 NFs+Pt/C-based Zn-air battery with other Co-based batteries reported before.

Catalyst	Electrolyte	Power density ($mW\ cm^{-2}$)	Ref.
CoS/Co_3O_4 NFs+Pt/C	6 M KOH+0.2 M $ZnCl_2$	127.9	This work
RuO_2+ Pt/C	6 M KOH+0.2 M $ZnCl_2$	102.6	This work
Eu_2O_3-Co/NC	6 M KOH+0.2 M $ZnCl_2$	123.3	[14]
NiCoFeP-HN + Pt/C	6 M KOH+0.2 M $ZnCl_2$	109	[15]
Pd/FeCo	6 M KOH+0.2 M $Zn(Ac)_2$	117	[16]
Fe-Co_4N@N-C	6 M KOH+0.2 M $Zn(Ac)_2$	105	[17]
Co/Co_3O_4@PGS	6.0 M KOH	118.27	[18]
NiO/CoN PINWs	6.0 M KOH	79.6	[19]

References

1. G. Kresse and J. Furthmüller, *Phys. Rev. B*, 1996, **54**, 11169-11186.
2. G. Kresse and J. Furthmüller, *Comp. Mater. Sci.*, 1996, **6**, 15-50.
3. G. Kresse and D. Joubert, *Phys. Rev. B*, 1999, **59**, 1758-1775.
4. H. J. Monkhorst and J. D. Pack, *Phys. Rev. B*, 1976, **13**, 5188-5192.
5. S. Grimme, S. Ehrlich and L. Goerigk, *J.Comp. Chem.*, 2011, **32**, 1456-1465.
6. S. L. Dudarev, G. A. Botton, S. Y. Savrasov, C. J. Humphreys and A. P. Sutton, *Phys. Rev. B*, 1998, **57**, 1505-1509.
7. H. Luo, W. J. Jiang, S. Niu, X. Zhang, Y. Zhang, L. P. Yuan, C. He and J. S. Hu, *Small*, 2020, **16**, e2001171.
8. P. He, X. Y. Yu and X. W. Lou, *Angew. Chem. Int. Ed. Engl.*, 2017, **56**, 3897-3900.
9. X. Yuan, H. Ge, X. Wang, C. Dong, W. Dong, M. S. Riaz, Z. Xu, J. Zhang and F. Huang, *ACS Energy Let.*, 2017, **2**, 1208-1213.
10. Z.-H. Xue, H. Su, Q.-Y. Yu, B. Zhang, H.-H. Wang, X.-H. Li and J.-S. Chen, *Adv. Energy Mater.*, 2017, **7**, 1602355.
11. Y.-W. Lee, J.-Y. Lee, D.-H. Kwak, E.-T. Hwang, J. I. Sohn and K.-W. Park, *Appl. Catal. B: Environ.*, 2015, **179**, 178-184.
12. Y. Kang, F. Li, S. Li, P. Ji, J. Zeng, J. Jiang and Y. Chen, *Nano Res.*, 2016, **9**, 3893-3902.
13. K. Mandal, D. Bhattacharjee, P. S. Roy, S. K. Bhattacharya and S. Dasgupta, *Appl. Catal. A: Gen.*, 2015, **492**, 100-106.
14. B. Guenot, M. Cretin and C. Lamy, *J. Appl. Electrochem.*, 2015, **45**, 973-981.
15. Z.-Y. Zhou, S.-J. Shang, N. Tian, B.-H. Wu, N.-F. Zheng, B.-B. Xu, C. Chen, H.-H. Wang, D.-M. Xiang and S.-G. Sun, *Electrochem. Commun.*, 2012, **22**, 61-64.
16. X. Shi, Y. Wen, X. Guo, Y. Pan, Y. Ji, Y. Ying and H. Yang, *ACS Appl. Mater. Interfaces*, 2017, **9**, 25995-26000.
17. X. Li, H. Hodson, C. Batchelor-McAuley, L. Shao and R. G. Compton, *ACS Catal.*, 2016, **6**, 7118-7124.
18. Z.-Y. Shih, C.-W. Wang, G. Xu and H.-T. Chang, *J. Mater. Chem. A*, 2013, **1**, 4773-4778.
19. J. Yin, Y.-X. Li, F. Lv, Q.-H. Fan, Y.-Q. Zhao, Q.-L. Zhang, W. Wang, F.-G. Cheng, P.-X. Xi and S.-J. Guo., *ACS Nano* 2017, **11,** 2275−2283.